Investigation of Cold Extrusion of Aluminum AA 2024 Alloy using Finite Element Analysis

Anupama Francy KOTHASIRI*,[1,a], Srinivasa Rao CHALAMALASETTI[2,b]

*Corresponding author
*,[1]Vishnu Institute of Technology, Bhimavaram, West Godavari,
Andhra Pradesh, India, Pin code 534202,
anupamafrancy.k@vishnu.edu.in
[2]Andhra University College of Engineering, Visakhapatnam,
Andhra Pradesh, India, Pin code 530003,
csr_auce@yahoo.co.in

DOI: 10.13111/2066-8201.2022.14.3.14

Received: 26 January 2022/ Accepted: 01 August 2022/ Published: September 2022

Abstract: *In recent years, the interest in modeling extrusion processes has resulted in the development of several analytical and numerical methodologies. The present work optimizes cold extrusion process variables (Die angle (DA), Ram speed (RS), Coefficient of friction (CoF)) on extrusion force, displacement, damage and time for the Aluminum AA 2024 alloy material. DEFORM^{TM}-3D software is used to carry out numerical simulations and to study the behavior of the Aluminum AA 2024 billet during the plastic deformation over the conical die. The die/ container and ram (top die) are considered as rigid bodies and the room temperature is maintained during the extrusion process. The simulations are conducted as per L_{27} Taguchi orthogonal array. The obtained results are analyzed in ANOVA. An optimization using multiple variables is performed by grey relational analysis (GRA). The highest grey relational grade (GRG) is obtained for experiments conducted at DA level 2, RS level 2, and CoF level 3 (minimum extrusion force, damage and time) and (maximum displacement) is achieved by GRA. Systematically, the influence of the ram speed, coefficient of friction, and die angle are examined. The damage factor is considerable at 30°DA under the ram speed of 3mm/min.*

Key Words: *DEFORM^{TM}-3D, Die Angle, Stress Distribution, Extrusion Force and Damage*

1. INTRODUCTION

Aluminum was designated as "the new millennium's metal" in recent years. Extruded Aluminum is extensively used in aerospace, construction and automotive industries [1&2]. Extrusion is a process that uses a hydraulic press to force a round workpiece through a die in order to mold it into the required shape. The induced compression and shear forces lead the stress to build until it reaches the plastic flow that occurs through the die. Cold and hot extrusions are two different types of extrusion processes. The cold extrusion procedure has the extra benefit of having better mechanical properties than the hot extrusion method [3]. The advances in and review of the cold extrusion process are explained briefly [4].

[a] Associate Professor
[b] Professor

Although the method of extrusion process appears to exist straightforward, it significantly depends upon the geometrical parameters such as die angle, ram speed, material, die land height, extrusion ratio, shape of the product, coefficient of friction and cross-sectional area [5&6]. A porthole die made of thin-walled extrusion profiles, is used to evaluate stress variations and extrusion pressure. The extrusion force was raised until it reached the extreme die angle of 80° and thereafter it abruptly decreased to zero at 110° due to the substantial distortion that occurs at higher die angles [7&8]. Area reduction, die angle and friction impact are considered influencing factors on central bursting defects in products [9]. To examine the core bursting flaws in the rod extrusion process, the upper bound limit analysis is used. Additional comparisons are made between the findings of the finite element simulation results.

The friction factor significantly influences the extrusion power limit in both cold and hot extrusion methods. A straightforward/simple numerical method based on the lubrication approximation is suggested for identifying the best die design. Using a set of extrusion variables, Taguchi orthogonal array L_9 is planned to conduct the experimental results in finite element analysis [10]. Along with other extrusion parameters, ram speed is used as an input process variable. Extrusion force increases as punch speed increases, as higher punch speeds result in higher flow stress and complicated strain rates. Because ram speed has the greatest impact on the extrusion force, and we observed that it is one of the crucial factors [11&12].

As manufacturing grows, the simulation capabilities advances, designers can now use computer-aided design to increase accuracy, reduce design time, and increase tolerance at every stage of the process [13]. The effect of extrusion ratio and die angle on the extrusion force is examined quantitatively by Venketesan et al [14]. Sadollah et al. [15] use the simulated annealing optimization method to minimize the extrusion force. Friction, logarithmic strain, and die angle characteristics are all taken into account in their studies. Considering the die cone angle and extrusion die ratio as influence variables, Tapas et al. [16] used round and square dies to minimize the extrusion force for the Al 6061 alloy material at reduction ratios of 20:1 and 60:1. The extrusion pressure and extrusion force are significantly predicted by diameter and strain. The regression technique is used to obtain mathematical formulas for force and pressure[17]. The velocity vector is used to examine the metal flow law of the part in the cold extrusion process, and the Deform-3D programme is used to minimize the extrusion forming process of the connecting screw [18].

Experiments are performed to identify effective die entrance angles for materials like Aluminum, in order to calculate the lowest extrusion force [19]. BN reinforced metal matrix composites based on Al 6061 were created and then put through the extrusion process. Both before and after the extrusion process, tests on the mechanical properties (hardness and tensile strength) are conducted. When compared to cast composites, extruded composites show improvements in hardness of up to 12% and tensile strength of up to 7% [20]. A cast Al-8Mg alloy was subjected to extrusion process at different zones and was studied experimentally. The highest hardness is obtained at middle zone of the workpiece and it was increased after the first pass of the process. From the experimentation it was observed that both yield strength and micro hardness increased with the number of passes [18]. Mechanical properties and metallurgical samples of Cu alloy (Zn-0.7, Mg-3.0, Zr-1.0) are examined earlier and later during the extrusion process. After the extrusion process, the hardness improved by 30% in the samples [21]. The relationship between hardness and strain value is consistent with the authors' previous findings.

Commercial and military aircraft, as well as Navy ships and aircraft (wing and fuselage) structures, frequently use Aluminum AA 2024 material [22, 23]. According to the literature, the key process variables like extrusion ratio, die angle, coefficient of friction, and ram speed

have a considerable impact on extrusion output characteristics. The deformation behavior (load-punch displacement curves) of Aluminum AA 2024 alloy has significant effect on the process parameters of the cold forward rod extrusion and the available studies have not yet addressed it. Some of the studies available in the open literature revealed that only one output response was considered. So, in the present work, the impact of these parameters (die angle, coefficient of friction, and ram speed) and optimization on these extrusion process parameters is investigated experimentally and numerically. Extrusion force, damage, displacement and time are the main output characteristics considered in these investigations. For multiple optimization, the GRA approach is used.

2. SLAB METHOD FOR EVALUATION OF EXTRUSION FORCE

Siebel developed a theory known as Slab theory based on elementary plasticity for the purpose of force calculation. This theory is used for Industrial purposes. The total deformation work (P_{tot}) on the deformed element can be obtained by considering deriving expressions of deformation forces for ideal (P_{id}), friction (P_{fr}) and shearing (P_{sh}) on the element. The various forces acting on the element are shown in Fig. 1. In terms of force is:

$$P_{tot} = P_{id} + P_{fr} + P_{sh} \tag{1}$$

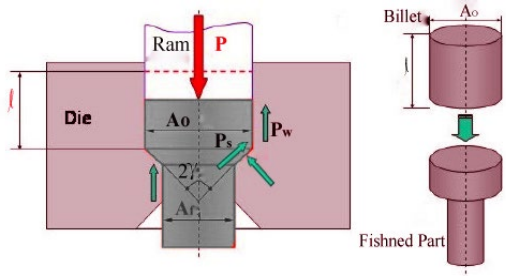

Fig. 1 – Forces acting on the work piece

Step 1: In the solid forward extrusion, first the ideal deformation force P_{id} was calculated:

$$dW_{id} = \Delta z dA\sigma_r + A\, d\Delta z\sigma_z \tag{2}$$

Using the yield condition and integrating between - original area and the final area, the ideal deformation work becomes:

$$W_{id} = V\sigma_{f,m}\, \emptyset_{\max} \tag{3}$$

Step 2: The frictional force for solid forward extrusion process consists along the die wall and on the shoulders of the die.

Consider a disk–shaped volume element in the shoulder having a cross-section A, a mean circumference $S = \pi d$, and a disk thickness ΔS, the disk is moved by ΔZ in the flow direction. The frictional force is given by

$$dW_{fr,s} = \mu\sigma_f \frac{\pi d\Delta S}{cos\gamma}\left[\frac{dz}{cos\gamma}\right] \tag{4}$$

And integrating between the areas of the original-cross section and final cross-section, the total frictional work on the shoulder is given by

$$W_{fr,s} = V.\sigma_{fm}.\phi_{max}\frac{2\mu}{sin2\gamma} \tag{5}$$

Step 3: The shearing work W_{sh} for small angles is given by

$$dW_{sh} = \frac{1}{2}\sigma_f \gamma dv \tag{6}$$

The volume element dV can be calculated as

$$dV = 2\pi r.\Delta S.dr \tag{7}$$

Integrating equation (5) by substituting equation (6)

$$\Delta W_{sh} = \int_0^{r_0} \frac{1}{2}\sigma_f.\frac{r}{s}2\pi r.\Delta S.dr \tag{8}$$

The total shearing work is obtained.

$$W_{sh,tot} = \frac{2}{3}V\gamma\sigma_f \tag{9}$$

The total work done in the solid forward extrusion process is

$$\frac{W}{V} = \frac{P}{A_{orginal}} \tag{10}$$

The force P is given by

$$\frac{W_{tot}}{V} = \sigma_{f,m}\left[\frac{2}{3}\gamma + \left(1 + \frac{2\mu}{sin^2\gamma}\right)\phi_{max}\right] + \frac{1}{2}\pi d_0 \mu \sigma_f (l_0^2 - l^2) \tag{11}$$

$$P = A_{original}\sigma_f\left[\frac{2}{3}\gamma + \left(1 + \frac{2\mu}{sin^2\gamma}\right)\phi_{max}\right] \tag{12}$$

The frictional force along the container wall should be added to P then above equation becomes

$$P_{fr,w} = \pi d_0 l.\mu.\sigma_f \tag{13}$$

After substituting equations (3), (5), (9), (11) and (13) in equation (1) the following equation (13) obtained.

$$P_{tot} = A_{orginal}\sigma_f\left[\frac{2}{3}\gamma + \left(1 + \frac{2\mu}{sin^2\gamma}\right)\phi_{max}\right] + \pi d_0 l\mu\sigma_f \tag{14}$$

where σ_f is the flow stress, γ is the die angle, l is the length of the billet, μ is the coefficient of friction, $A_{orginal}$ is the original area of the billet and d_0 is the billet diameter.

3. MATERIAL AND METHODOLOGY

In this study, the work flow can be divided into three primary parts. The first step involves selecting the workpiece material and extrusion process impacting the input parameters. The simulation matrix is created using the Taguchi method in the second stage, and the simulation is performed by DEFORM™-3D software. The last step, Taguchi and Grey algorithms are used for optimization, based on the results of the simulation. The following section completely describes each stage in great depth.

3.1 Selection of Material for the Extrusion Process

Aluminum AA 2024 alloy is employed as the billet (workpiece) material for this simulation. It is a cost-effective material with good physical properties (Density 2.78 g/cm^3, Young's Modulus 73.1 GPa, Tensile yield strength 324 MPa, and Poisson's ratio 0.33), as well as a

good surface finish and corrosion resistance [24]. As a result, Aluminum AA 2024 alloy is widely utilized in applications such as navy ship building, aircraft structures, particularly wing and fuselage structures, commercial and military aircraft, and so on [26].

Table 1 shows the chemical composition of the Aluminum AA 2024 alloy material. H13 steel is used for the die and ram [27]. Table 2 shows the chemical composition and physical parameters of H13 steel.

Table 1 – Composition Elements of AA 2024 billet material [24 & 25]

Element	**Fe**	**Cu**	**Zn**	**Si**	**Cr**	**Mg**	**Mn**	**Ti**	**Al**
Composition (wt. %)	0.51	4.0	0.25	0.5	0.1	1.5	0.5	0.15	94.7

Table 2 – H13 steel elemental composition for die [27]

Chemical Composition										
Element	**Mn**	**Cr**	**Mo**	**V**	**C**	**Ni**	**P**	**Cu**	**S**	**Si**
Composition(wt.%)	0.40	5.25	1.36	1.01	0.41	0.30	0.031	0.251	0.0311	1.01
Physical Properties										
Density	**Melting point**			**Youngs Modulus**				**Poisson's ratio**		
7.81 g/cm^3	1426°C			214 GPa				0.28 - 0.30		

3.2 Modelling and Simulation Matrix

Taguchi and Konishi [13] formulated a model for optimizing many variables with a number of objectives. This strategy is successfully used to plan the simulation matrix in the current study. Major influencing parameters play an important role in this procedure, which is employed to attain optimal levels of the process variables for the development of quality features. Practice an orthogonal array (OA), which uses the least amount of simulation to learn the full range of process parameters. Table 3 provides a list of the levels of the input parameters chosen for the present study. S/N ratio stands for the measure of quality features in Taguchi optimization and is calculated as follows.

$$\frac{S}{N} = \eta = -10\log_{10}\left[\frac{1}{n}\sum_{i=1}^{n} y_i^2\right] \tag{15}$$

$$\frac{S}{N} = \eta = -10\log_{10}\left[\frac{1}{n}\sum_{i=1}^{n} \frac{1}{y_i^2}\right] \tag{16}$$

For smaller S/N ratio Eq. 15 is used and for larger S/N ratio Eq. 16 is better. The S/N ratio is computed for damage, extrusion force, and time is by applying smaller-is-better criterion, to reduce extrusion force, damage and time.

The S/N ratio is calculated for billet displacement by applying the larger-is-better criterion, to maximize the displacement. Table. 4 presents the OA simulation matrix utilizing the Taguchi technique in detail.

Table 3 – Extrusion Parameters according to the levels

Factor symbol	**Factors**	**Level 1**	**Level 2**	**Level 3**
DA	Die Angle (deg)	10	20	30
RS	Ram Speed (mm/min)	1	2	3
CoF	Coefficient of Friction	0.06	0.08	0.1

Table 4 – Design of simulation using L_{27} orthogonal array

Exp.no	DA	RS	CoF	Extrusion Parameters			Extrusion Force (kN)	
				Damage (%)	Displacement (mm)	Time (Min)	Deform-3D	Slab Method
1	1	1	1	0.15	25.79	7.67	601	630
2	1	1	2	0.11	25.89	7.58	616	636
3	1	1	3	0.11	25.92	7.61	630	640
4	1	2	1	0.15	25.84	6.87	633	643
5	1	2	2	0.36	25.89	6.52	638	650
6	1	2	3	0.19	25.94	6.36	640	652
7	1	3	1	0.01	25.89	5.89	643	692
8	1	3	2	0.01	25.92	5.81	648	696
9	1	3	3	0.09	25.99	5.69	681	697
10	2	1	1	0.26	25.79	5.75	790	802
11	2	1	2	0.01	25.87	5.54	796	805
12	2	1	3	0.3	25.95	5.48	800	808
13	2	2	1	0.36	26.17	5.04	802	827
14	2	2	2	0.65	26.21	4.88	808	827
15	2	2	3	0.01	26.4	4.8	810	827
16	2	3	1	0.41	26.58	4.27	814	840
17	2	3	2	0.43	26.65	3.91	824	843
18	2	3	3	0.37	26.75	3.84	829	846
19	3	1	1	1.88	26.15	3.89	1001	1016
20	3	1	2	0.81	26.2	4.19	1006	1020
21	3	1	3	2.18	26.25	3.86	1009	1023
22	3	2	1	1.73	26.69	3.71	1010	1031
23	3	2	2	0.77	26.78	3.5	1012	1033
24	3	2	3	2.25	26.89	3.28	1019	1037
25	3	3	1	1.79	27.11	3.06	1022	1038
26	3	3	2	2.73	27.3	2.94	1024	1040
27	3	3	3	2.75	27.25	1.88	1028	1045

3.3 Simulation Procedure – DEFORM^{TM}- 3D

For the current investigation, DEFORM^{TM}-3D V6.1 software is used to run FEM simulations. Pre-processor, simulation engine system, and post-processor are the three key modules of the DEFORM^{TM}-3D system.

CATIA software is used to model the die, workpiece, and punch tool. The models (die, workpiece and punch) are then transferred to DEFORM^{TM}-3D in the format of STL. The material flows at various steps during the simulations and are shown in Fig. 2.

The properties of the material are selected from the data base software for simulation. A finite element mesh is completed approximately through 1800 nodes and 180000 elements.

A uniform mesh size is maintained to all the experiments. The Lagrangian increment is applied to a four-node tetrahedral element. The non-linear simulation equations are solved using the Newton-Raphson method.

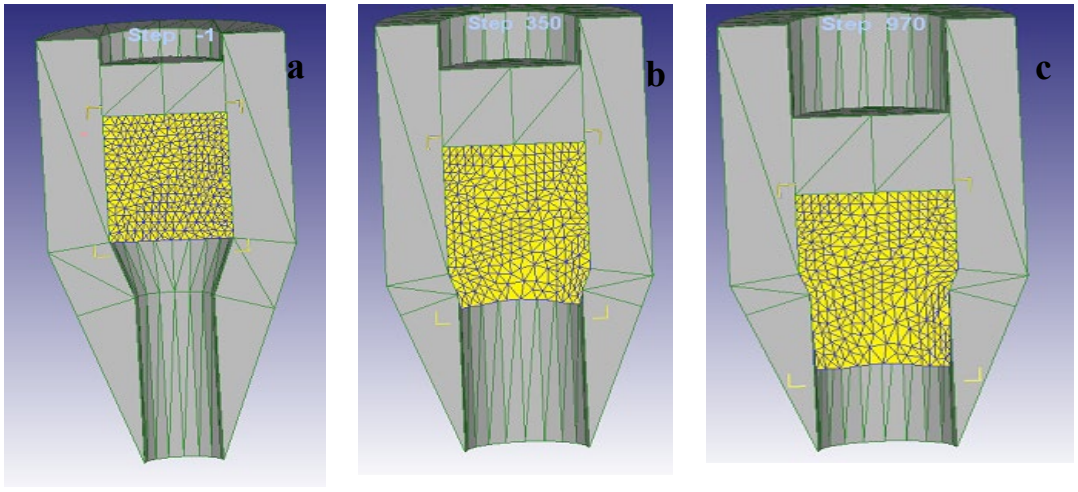

Fig. 2 – Material flow at various steps during the simulation for 30° die angle (a) Step-1, (b) Step-350, (c) Step-970

3.4 Grey Relational Analysis for Optimization Of Extrusion Process Parameters

In multi-objective optimization problems, the grey relational technique is often utilized. This approach solves issues with the interrelationship of many variable optimization. This article goes into detail about the GRA optimization process.

Evaluation of the S/N ratio using simulated data ranging from 0 to 1 is the first stage by using Eq. 15 and 16.

Following the Grey Relation Normalization, the Grey Relational Coefficient (GRC) and the Resolve of Grey Relational Grade (GRG) need to be assessed.

The estimation of the grey relational normalization for the lower-the-better condition is done using the standardized data of the extrusion force, damage, and time from the simulation. and is given in Eq. 17.

$$x_i(l) = \frac{\max y_i(l) - y_i(l)}{(\max y_i(l) - \min y_i(l))} \tag{17}$$

The next step is to determine the Grey relationship coefficient after normalizing the new order $\varepsilon_i(l)$.

$$\varepsilon_i(l) = \frac{\Delta_{\min} + \varphi\, \Delta_{\max}}{\Delta_{oi}(l) + \varphi\Delta_{\max}} \tag{18}$$

where $\Delta_{oi} = \|x_o(l) - x_i(l)\|$ = a total value change $x_o(l)$ and $x_i(l)$; φ is a separate coefficient. The average response of each grey relational coefficient is known as the grey relational grade. Estimates of the grey relational grade β_i are possible by Eq.16 and is given below.

$$\beta_i = \frac{1}{m}\sum_{l=1}^{m} \varepsilon_i(l) \tag{19}$$

m indicates the quantity of the process responses.

The simulation findings in the current work are standardized directly. Extrusion force, damage, displacement, and time are the best output parameters.

Since the simulation, every response has been regulated in a 0 to 1 scale, which referred to as Grey relational coefficient.

The response variables of S/N Ratio for the extrusion force, damage, displacement and time are shown in Table 5.

Table 5 – S/N Ratio, GRC and GRG for L_{27} orthogonal array

Exp. no	S/N Ratio				Gray Relational Coefficient				GRG
	Force	Damage	Displacement	Time	Force	Damage	Displacement	Time	
1	55.58	-16.48	-28.29	17.70	1.00	0.52	0.35	0.33	0.55
2	55.79	-19.02	-28.29	17.59	0.92	0.55	0.35	0.34	0.54
3	55.99	-18.86	-28.29	17.63	0.85	0.54	0.35	0.34	0.52
4	56.03	-16.48	-28.30	16.74	0.84	0.52	0.36	0.35	0.52
5	56.10	-8.87	-28.30	16.29	0.82	0.44	0.36	0.36	0.50
6	56.12	-14.43	-28.30	16.07	0.81	0.49	0.36	0.37	0.51
7	56.16	-38.79	-28.27	15.40	0.80	1.00	0.34	0.38	0.63
8	56.23	-36.95	-28.27	15.28	0.78	0.93	0.34	0.38	0.61
9	56.66	-21.31	-28.27	15.10	0.68	0.58	0.34	0.39	0.50
10	57.95	-11.70	-28.28	15.19	0.50	0.47	0.35	0.39	0.43
11	58.02	-38.13	-28.28	14.87	0.49	0.97	0.35	0.39	0.55
12	58.06	-10.46	-28.28	14.78	0.48	0.46	0.35	0.40	0.42
13	58.08	-8.80	-28.55	14.05	0.48	0.44	1.00	0.42	0.59
14	58.15	-3.74	-28.55	13.77	0.48	0.40	1.00	0.42	0.58
15	58.17	-38.79	-28.55	13.63	0.47	1.00	1.00	0.43	0.73
16	58.21	-7.39	-28.32	12.61	0.47	0.43	0.38	0.46	0.44
17	58.32	-7.45	-28.32	11.84	0.46	0.43	0.38	0.49	0.44
18	58.37	-8.66	-28.32	11.69	0.46	0.44	0.38	0.50	0.44
19	60.01	5.48	-28.38	11.80	0.35	0.35	0.46	0.49	0.41
20	60.05	-1.81	-28.38	12.44	0.34	0.39	0.46	0.47	0.42
21	60.08	6.77	-28.38	11.73	0.34	0.34	0.46	0.49	0.41
22	60.09	5.06	-28.26	11.39	0.34	0.35	0.33	0.51	0.38
23	60.10	-2.27	-28.26	10.88	0.34	0.39	0.33	0.53	0.40
24	60.16	7.04	-28.26	10.32	0.34	0.34	0.33	0.56	0.39
25	60.19	1.06	-28.30	9.71	0.34	0.37	0.37	0.59	0.42
26	60.21	8.72	-28.30	9.37	0.34	0.33	0.37	0.61	0.41
27	60.24	8.79	-28.30	5.48	0.33	0.33	0.37	1.00	0.51

Table 5 shows the S/N Ratio, grey relational coefficients (GRC) and grey relational grade (GRG) of output values. Grey Relation coefficients after weighted and grey relational grades for every experiment by L_{27} orthogonal array is tabulated.

Among 27 experiments, experiment 15 has best multiple performance characteristics because it has the highest grey relation grade.

To accurately estimate the ideal combination set of process parameters, it is still necessary to understand the significance of the extrusion process parameters on the numerous performance characteristics.

4. RESULTS AND DISCUSSIONS

The influence of the process parameters (DA, RS and CoF) on displacement, time, extrusion force and damage are investigated numerically.

As previously defined, the Taguchi L_{27} orthogonal array approach is used to design a total of 27 simulations.

Simulations are executed in DEFORM^{TM}-3D software and some of the observations are explained in detail. Minitab software is used to perform the ANOVA analysis.

4.1 Influence of extrusion parameters on extrusion force

Table 6 lists the effects of the process variables (DA, RS, and CoF) on extrusion force. The results depict that the increase of die angle enhances the extrusion force.

The CoF influence on extrusion force is negligible. According to the findings of the ANOVA, the die angle has the largest significance (99.09 %), followed by the ram speed (0.59%), and then by the coefficient of friction (0.14%).

Table 6 –Analysis of Variance on Extrusion Force

Source	DoF	Adj ss	Adj ms	f-value	p-value	% of cont.
DA	2	644438	322219	6159.66	0	99.0975
RS	2	3878	1939	37.07	0	0.5963
CoF	2	945	472	9.03	0.002	0.1453
Error	20	1046	52			
Total	26	650307				

Figure 3 shows the prediction of the load-stroke plot for 20° die angle and 30° die angle under different extrusion conditions.

Similar kind of graph has been observed for 10° die angle also. The graph shows that, the extrusion force increases from the initial position to certain value till the die completely filled with the billet.

Then the extrusion force becomes stable until it reaches the maximum value. This increasing force is obtained by strain and strain hardening effect. Extrusion force increases with increment of the die angle from 10° to 30°.

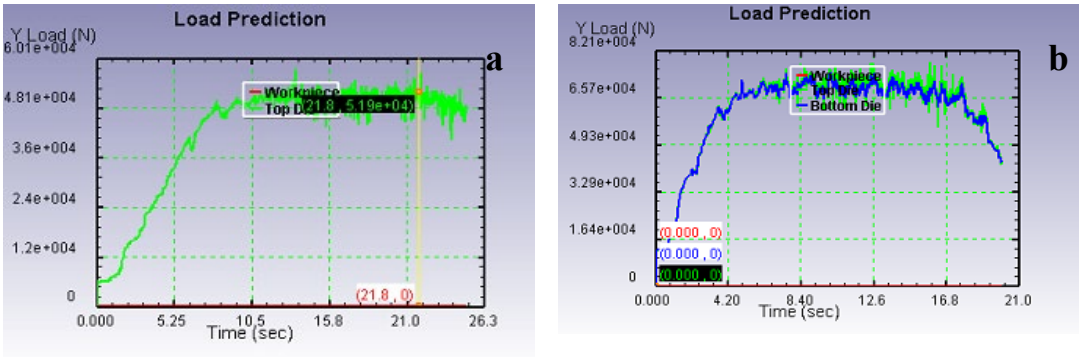

Fig. 3 – Prediction of load-stroke plots at various die angles. (a) 20°die angle, (b) 30°die angle

The effective stress distributions across the billet at the various stages of the extrusion process at 10° and 30° under different conditions from the post processor result analysis are

shown in Fig 4. It is clearly observed from the figure that, the effective stress increases as the die angle increases from 10° to 30°.

The maximum effective stress is developed in the billet where the billet has just begun from the conical die and at the corners. The effective stress increases from 363 MPa to 387 MPa over the die angles of 10° to 30°.

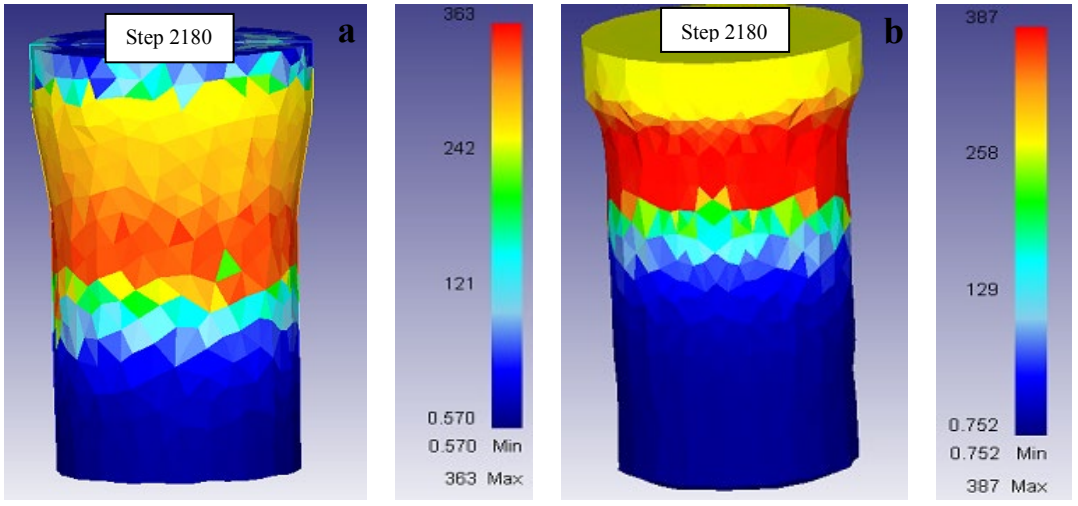

Fig. 4 – Effective stress distribution from the post – processor analysis (a) 10° die angle, (b) 30° die angle

4.2 Influence of extrusion parameters on displacement

Table 7 provides the effects that the process variables (die angle, ram speed, and CoF) have on displacement.

According to the ANOVA results, die angle (54.69%) and ram speed (30.29%) both has a significant impact.

After extrusion, the workpiece displacement at 10° and 30° die angles at 3 mm/min is illustrated in Fig. 5.

The maximum displacement takes place for 30° die angle than 20° & 10°die angles. Displacement increases with increasing of the die angle and ram speed.

The displacement increases from 25.9 mm to 27.3 mm for die angle ranging from 10° to 30°.

Table 7 – Analysis of Variance for Displacement

Source	DoF	Adj ss	Adj ms	f-value	p-value	% of cont.
DA	2	3.1835	1.5918	41.07	0	54.6946
RS	2	1.7635	0.8817	22.75	0.037	30.2974
CoF	2	0.0984	0.0492	1.27	0.303	1.6899
Error	20	0.7752	0.0388			
Total	26	5.82054				

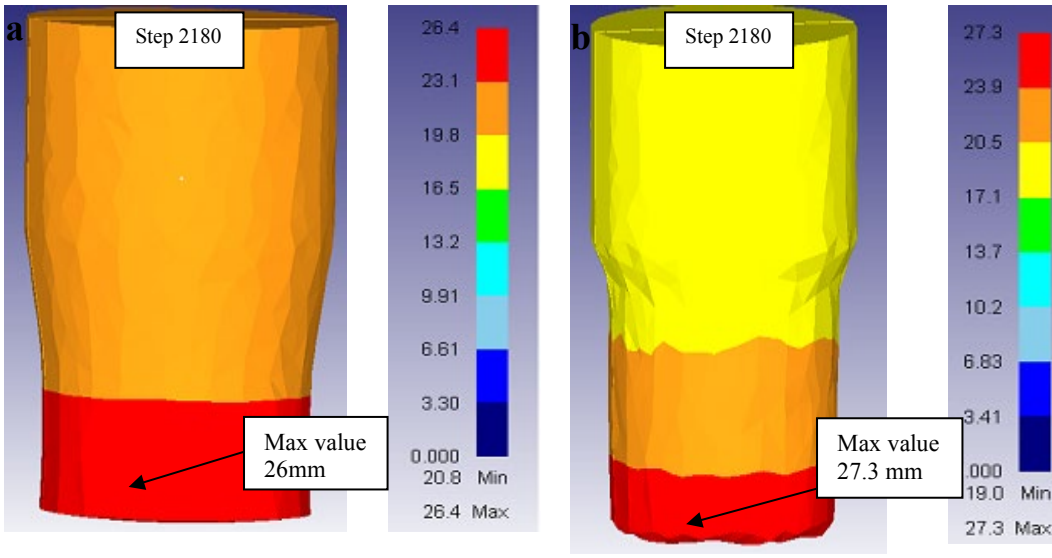

Fig. 5 – Displacement of the billet after the extrusion process at a ram speed of 3 mm/min. (a) 20° die angle, (b) 30° die angle

4.3 Influence of extrusion parameters on damage

The influence of the process parameters (die angle, ram speed and CoF) on damage factor are quoted in Table 8.

From the ANOVA results, it is observed that die angle has highest significance (78.54%) followed by ram speed (2.22%) and followed by the coefficient of friction (1.51%).

Figure 6 shows that the value of damage distribution over the surface of the billet is observed for 20° and 30° die angle at the same ram speed of 3mm/min. The damage occurs at 30°die angle for a ram speed of 3mm/min and no damage is observed for 30° die angle at ram speed of 2mm/min and friction condition 0.1.

It is observed that the maximum damage distribution occurs on the surface of the billet after certain displacement from the exit region.

This critical damage occurs because of the maximum tensile stress at a point on the billet surface.

The damage value increases with increasing of the die angle and maximum stress. Damage value increases from 0.15% to 2.75% as the die angles increases from 10° to 30°. In the extrusion process, the conical die performs like a stress raiser.

Table 8 – Analysis of Variance for Damage

Source	DoF	Adj ss	Adj ms	f-Value	p-Value	% of cont.
DA	2	16.591	8.2955	44.33	0	78.5484
RS	2	0.4688	0.2344	1.25	0.307	2.2195
CoF	2	0.3199	0.1599	0.85	0.44	1.5145
Error	20	3.7423	0.1871			
Total	26	21.122				

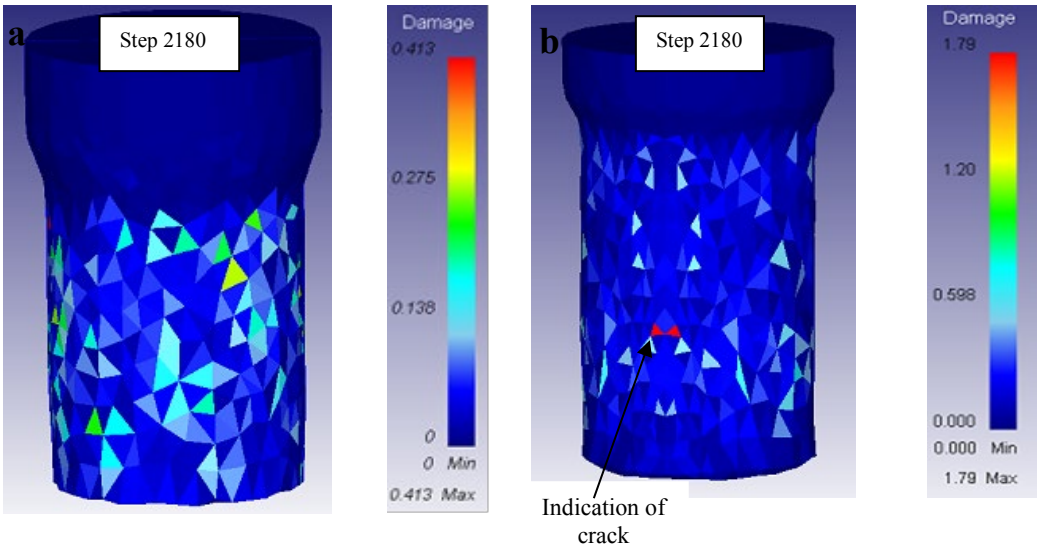

Fig. 6 – Damage distribution over the surface at a ram speed of 3 mm/min. (a) 20° die angle, (b) 30° die angle

4.4 Influence of extrusion parameters on time

Table 9 provides the effects of the process parameters (die angle, ram speed, and CoF) on time. According to the ANOVA results, the die angle has a higher significance (79.13%) than the ram speed (18.26%) and is followed by the coefficient of friction (1.02%). Results revealed that the die angle and ram speed show a significant effect on decreasing time. Increasing of die angle and ram speed decreases extrusion time.

Table 9 – Analysis of Variance for Time

Source	DoF	Adj ss	Adj ms	f-value	p-value	% of cont.
DA	2	49.1725	24.5862	502.3	0	79.1369
RS	2	11.3496	5.6748	115.94	0	18.2657
CoF	2	0.635	0.3175	6.49	0.007	1.0220
Error	20	0.9789	0.0489	-	-	-
Total	26	62.136	-	-	-	-

4.5 Influence of extrusion parameters on GRG

Grey Relational Grade (GRG) optimizes the extrusion process settings based on the results of simulations. Table 10 provides the effects of process variables (die angle, ram speed, and CoF) on GRG.

Table 10 – Analysis of Variance for GRG

Source	DoF	Adj ss	Adj ms	f-value	p-value	% of cont.
DA	2	0.0756	0.0378	6.85	0.005	39.2264
RS	2	0.0064	0.0032	0.58	0.571	3.3027
CoF	2	0.0004	0.0002	0.04	0.961	0.2284
Error	20	0.1103	0.0055	-	-	-
Total	26	0.192628	-	-	-	-

The GRG (the combined influence of extrusion force, damage, displacement and time) response behavior with the process parameters variation can be observed in Fig. 7. GRG decreases with the increase of process parameters DA, RS & CoF.

Based on the individual plots, it can be seen that DA and RS have a significant impact on extrusion force, displacement, and time.

In contrast, CoF has a negligible impact on the extrusion force and a modest impact on damage, time, and displacement.

Therefore, it is anticipated that the DA and RS will have a considerable impact on how the DA & RS contour is depicted. The influence on CoF's orientation is constant for the other contours it displays.

According to the DA and RS contour plot, there is a high GRG in the area between low DA (20° to 30°), low RS (2 mm/min). Similar to this, the GRG is high in the area that is bordered by the medium DA and high CoF (DA & CoF) and the medium & high CoF & medium RS (CoF & RS).

The ideal conditions for extrusion force, damage, displacement, and time (i.e. high GRG) are at 20° DA, 2 mm/min RS, and 0.1 CoF.

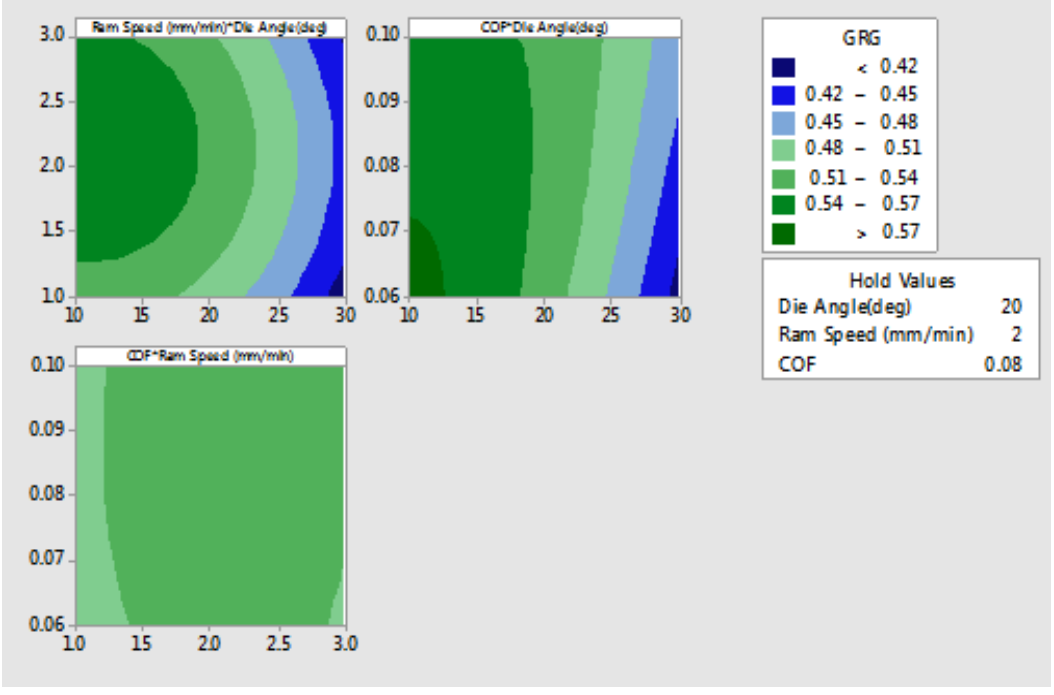

Fig. 7 – Contour plots of GRG

5. VALIDATION

The simulation data is used to validate the slab model employed in this investigation. The DA, CoF, and RS are all varied in the experiments.

Fig. 8 shows the variation of slab data and simulation data in terms of extrusion force. It has been proven that the existing simulation model/procedure predicts the extrusion force correctly.

Less than 5% of the measured average deviation is observed.

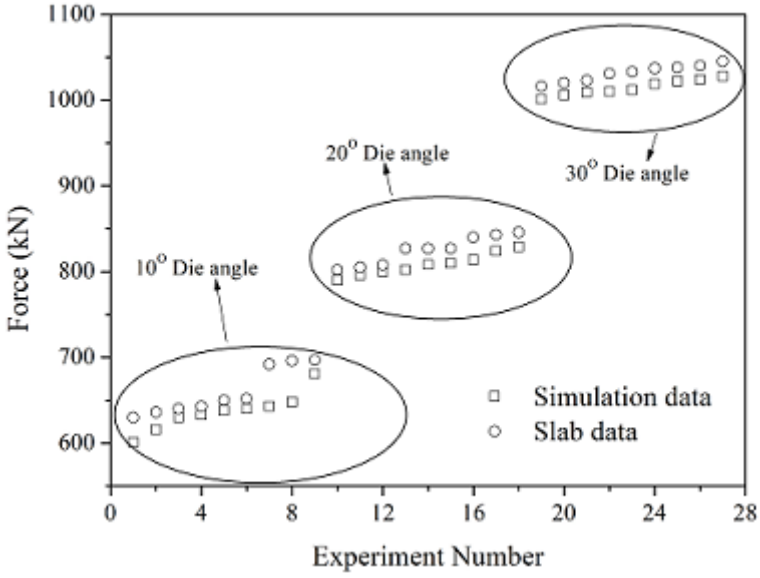

Fig. 8 – Comparisons of analytical and simulation results

6. CONCLUSIONS

The behavior of an Aluminum AA 2024 alloy workpiece during plastic deformation over a conical die is investigated in the current work using a finite element model (DEFORM^{TM}-3D software). The numerical results have been observed.

- With an enlarged die angle range of 10° to 30°, the extrusion force has been enhanced. The material flow during the deformation process is influenced by the die angle and ram speed. The extrusion force and product quality are influenced by the flow of the materials.
- Die angle shows highest significance in case of extrusion force and damage whereas ram speed shows considerable significance.
- After a specific distance from the die exit, the damage increases most on the outer surface of the billet. At 30° DA and ram speed of 3 mm/min, the damage is significant.
- Extrusion force and displacement increases as process parameters are increased and damage & time decreases with the increase of process parameters.
- As ram speed and die angle increase, the effective stress and effective strains increases as well.
- The displacement increases when the die angle and ram speed both increase at the same time, which causes the extruded component to be produced in less time.
- From the individual ANOVA analysis it is observed that DA and RS have a significant influence on extrusion force and displacement. CoF has a significant influence on damage and time.

Grey Relational Analysis is used to optimize the extrusion process parameters. The optimum combination of extrusion process parameters are obtained at 20° DA, 2 mm/min RS and 0.1 CoF respectively. The results revealed that, die angle, ram speed have a significant influence on extrusion force, damage and time and CoF shows less significance.

REFERENCES

[1] L. Deng, X. Wang, J. Jin, J. Xia, Precision forging technology for Aluminum alloy, *Frontiers of Mechanical Engineering*, **13**, pp:25-36, 2018, doi.org/10.1007/s11465-018-0477-y.

[2] Aluminum Extruders Council, Aluminum Extrusion, Manual, 4th ed. (USA): Aluminum Extruders Council and the Aluminum Association, 2018.

[3] L. Donati, B. Reggiani, R. Pelaccia, M. Negozio, S. Di Donato, Advancements in extrusion and drawing: a review of the contributes by the ESAFORM community, *Int. J. of Material Forming* **15**:41, 2022.

[4] N. Carvalho, A. Correia and F. de Almeida, The Evaluation of Defects in the Aluminium Extrusion Process through Quality Tools**,** *WSEAS Trans.Environ. Dev.* **14,** 1-15, 2018.

[5] L. Chen, G. Zhao, J. Yu, W. Zhang and T. Wu, Analysis and porthole die design for a multi-hole extrusion process of a hollow, thin-walled Aluminum profile, *Int J.Adv. Manuf.Technol*. **74**, 383-392, 2014.

[6] G. A. Chaudhari, S. R. Andhale, N. G. Patil, Experimental Evaluation of Effect of Die Angle on Hardness and Surface Finish of Cold Forward Extrusion of Aluminum, *Int J Emerg Technol Adv Eng*., **2**(7):2–6, 2012.

[7] D. Rath, S. Tripathy, Investigation of Extrusion of Lead experimentally from Round section through Equilateral Triangular section Converging dies at different area reductions during Forward Metal Extrusion Process, *International Journal Of Engineering And Science*, Vol. **3**, Issue 1 pp 32-38, 2013., 2013.

[8] S. O. Adeosun, O. I. Sekunow, O. P. Gbenebor, Effect of Die Entry Angle on Extrusion Responses of Aluminum 6063 Alloy, *International Journal of Engineering and Technology (IJET)*, **4**(2):127–34, 2014.

[9] A. Parghazeh, H. Haghighat, Prediction of central bursting defects in rod extrusion process with upper bound analysis method, *Trans. Nonferrous Met. Soc. China* **26**:2892−2899, 2016.

[10] S. M. Ali, To Study the Influence of Frictional Conditions and Die Land Length on Component Error and Die Deflection in Cold Extrusion by Finite Element Analysis, *J Metall Eng.*, **2**(1):29–38, 2013.

[11] B. Lela, A. Musa, O. Zovko, Model-based controlling of extrusion process, *Int J Adv Manuf Technol*., **74**(9–12):1267–73, 2014.

[12] S. I. Oh, W. T. Wu, J. P. Tang, Simulations of cold forging processes by the DEFORM system, *J Mater Process Tech*., **35**(3–4):357–70, 1992.

[13] Z. Jurković, M. Brezočnik, B. Grizelj, V. Mandic, Optimization of extrusion process by genetic algorithms and conventional techniques, *Teh Vjesn*., **16**(4):27–33, 2009.

[14] R. Venketesan, Extrusion Die profile Design using Simulated Annealing and Particle Swarm Optimization, *Int J Eng Sci Technol*., **2**(8):3758–61, 2010.

[15] A. Sadollah, A. Bahreininejad, Optimization of die design using metaheuristic methods in cold forward extrusion process, *Neural Comput Appl*., **21**(8):2071–6, 2012.

[16] F. Alfaqs, G. S. Marahleh, Force and Pressure Function Formulation for Direct Cold Extrusion of Aluminum Alloy Al 1350 Using Regression Method, *Naukovyi Visnyk Natsionalnoho Hirnychoho Universytetu*, pp:38-43, 2021, https://doi.org/10.33271/nvngu/2021-3/038.

[17] Y. Yuan, Y. Ren and Q. Wu, Research on Improvement of Cold Extrusion Technology of Connecting Screw, *Journal of Physics: Conference Series*, 2022, doi:10.1088/1742-6596/2160/1/012055

[18] T. Chanda, J. Zhou, J. Duszczyk, A comparative study on iso-speed extrusion and isothermal extrusion of 6061 Al alloy using 3D FEM simulation, *J Mater Process Technol*., **114**(2):145–53, 2001.

[19] V. R. Kargin and A. Y. Deryabin, Computer Simulation of Isothermal Forming Process of Aluminum-Alloy Figurine- Shaped panels, *Key Eng. Mater*. **684**, 211, 2016.

[20] Y. B. Mukesh, T. B.Bharathesh, R. Saravanan, R. K Eshavamurthy, Effect of hot extrusion on Mechanical behavior of boron nitride reinforced Aluminium 6061-based metal matrix composites, *Int. J. Materials Engineering Innovation*, vol. **10**, No.2. 2019.

[21] S. N. Gurugubelli, Extruded composites exhibit improvement in hardness up to 12% and tensile strength up to 7% in comparison with cast ones, *Int. J. Materials Engineering Innovation,* Vol. **7**, No. 1, 2016.

[22] Suneesh and M. Sivapragash, Effect of hot extrusion on the characteristics of an Mg-3.0Zn-0.7Zr-1.0 Cu alloy produced by powder metallurgy, *Int. J. Materials Engineering Innovation,* Vol. **11**, No.1, 2020.

[23] A. A. Akbar, R. S. Yaseen. Study of the Direct Extrusion Behavior of Aluminum and Aluminum Alloy-2014 Using Conical Dies, *Eng.&Tech. Journal*, **30**, 950 – 958, 2012.

[24] Z. Liu, P. H. Chong, A.N. Butt, P. Skeldon, Corrosion mechanism of laser-melted AA 2014 and AA 2024 alloys, *Applied Surface Science*, **247**:294–299, 2014.

[25] T. Sheppard, Extrusion of AA 2024 alloy, *Materials Science and Technology*, **9**, 430-440, 1993.

[26] A. F. Kothasiri, S. R. Chalamalasetti, G. Peteti, Multiple Process Parameter Optimization of Forward Extrusion Process on AA 2024, *Int. J. of Modern Manuf. Techn.*, Vol **XIII**, No. 2, pp.63-75, 2021.

[27] S. Jajimoggala, R. Dhananjay, V. V. K. Lakshmi, Shabana, Multi-response optimization of hot extrusion process parameters using FEM and Grey Relation bases Taguchi method, *Mat. Today: Proc.* (**18**) 38; 2019.